Article no. 29

THE CIVIL ENGINEERING JOURNAL 3-2018

STUDY ON A NEW DESIGN OF GROUTING PUMP FOR MANAGING WATER INRUSH IN KARST TUNNELS

Li Shucai, Li Mengtian[1], Zhang Xiao and Zhang Qingsong[1]

1.University of ShanDong, Research Center of Geotechnical and Structural Engineering, Jinan, 250061, China; 156207068@qq.com

ABSTRACT

The low flow rate and efficiency of existing grouting pumps such as piston pumps and diaphragm pumps result in difficulty in managing sudden water and slurry discharges. In this study, a new design for grouting pumps is proposed to improve the grouting flow rate and efficiency. A grouting model test scheme to manage the water inrush of a tubular karst is designed. The power consumption of this system is equivalent to that of a diaphragm grouting pump. Improved performance was also observed for the newly designed rotary piston pump in grouting plugging tests. The retention of slurry and changes in moving water flow are observed and recorded to examine the grouting effects of the pumps. In addition, the pressure and flow rate changes of the grouting slurry are used to gauge the performance parameters of the pumps. A rotary piston pump and a traditional piston pump were tested in single- and separate-hole grouting experiments in tunnel engineering sites. In the grouting model test, which manages the water inrush of a tubular karst, the newly designed rotary piston pump had a distinct advantage in terms of the slurry retention thickness and fracture sealing effect. In particular, the efficiency of the rotary piston pump increased by a factor of 10 over the diaphragm grouting pump. During the experiments in the engineering site, the grouting flow rate of the rotary piston pump showed significant increase when compared to the traditional piston pump. The construction time was halved. The proposed rotary piston grouting pump has shown obvious advantages over existing grouting pumps.

KEYWORDS

Karst water bursting, Grouting, Rotary piston pump, Grouting model test, Engineering field test

INTRODUCTION

In recent years, with the implementation of China's western development strategy, the construction of tunnels and underground infrastructure has gradually shifted to the southwest karst regions. When tunnels and underground works cross the karst areas, a sudden inrush of water often occurs. Such disasters endanger the personal safety of construction crews, delay the construction process, cause environmental hazards, and result in economic losses directly or indirectly [1-3].The process of karst water bursting can be divided into five different types according to the karst's spatial characteristics. These are, fissure type, small vessel type, pipe type, cave type and underground river type. The research focus of this article is on the pipe type bursting process, as it has become one of the main influencing factors in the underground engineering works in karst areas. Such areas are characterised by high flow rate, strong recharge and strong difference [4]. Water bursting in the karst tunnel fissures is the result of a split in a fractured rock mass disturbed by the underground construction while under the continuous pressure of the karst water [5]. After the excavation of the fissure, the internal filling medium is continuously lost, resulting in a pipe gush of the filling material. The soil extrudes as a whole, and the underground river water, cavity water or surface water flows into the tunnel. Eventually, the lining fractures and

the water bursts into the tunnel [1]. To manage such disasters, comprehensive advanced geological forecasting should be carried out. In addition, optimised treatment schemes aimed at preventing water bursting should be designed dynamically. Ultimately, the management and governance plans need to be established [6]. Grouting is an effective method to control the flooding in underground engineering. With recent advancements in engineering applications, the idea of "draining" is gradually changing towards "blocking" [7,8].

In any grouting project, the core equipment is the grouting pump. The performance of this pump is critical to achieve higher quality and efficiency in the construction project. The main types of grouting pumps available to date are piston pumps, diaphragm pumps and various reciprocating pumps, with piston pumps being the primary choice [9]. The piston pump is driven by a rod mechanism that is operated by a crankshaft rotation, which completes the reciprocating motion of the piston inside a cylinder. Although the sealing system is relatively perfect and operates well under higher pressure, the reciprocating motion of the piston can cause imbalance of inertia moment and inertia force. This may lead to an overload of inertia in the piston pump structure and cause unstable vibration and noise [10-12]. Moreover, the low flow rate of the piston type grouting pump causes reduced grouting efficiency. Several high-pressure and large-flow-rate plunger pumps have been designed and tested on test benches [13]. However, these pumps merely improve the bore size, and do not solve the fundamental problem.

In order to achieve the benefits of a high-pressure and high-flow type pump, a rotary piston pump is designed, which takes the advantage of the high pressure of a reciprocating pump and the high flow rate of a centrifugal pump. This is operated in the way of rotary extrusion. The rotary piston pump can be classified as a rotor pump, which has many commonalities with a typical rotor pump structure. However, the volumetric efficiency of most rotor pumps is low due to poor chamber sealing [14-17]. This paper presents the operating principle of the new grouting pump and design of a karst pipeline grouting test procedure. The CN-0.5S model is used to test the newly designed pump and a typical piston pump. The collected data were analysed and processed. Finally, the test flow rate, pressure, efficiency and other performance parameters were calculated [18-20].

GROUTING CONTROL TEST ON PIPELINE WATER BURSTING IN KARST AREA

In the control treatment of sudden flooding in a karst area by grouting, the grouting pump injects the slurry into the stratum medium. The slurry blocks the groundwater runoff and influx mainly by filling the cave cavity, karst pipeline, fissure passage and other water storage structures. With a continuous pumping and curing of the slurry, the overcurrent cross-sectional area of the burst water gradually decreases. The diffusion resistance of the slurry gradually increases. In other words, the damping property of the injected formation medium gradually increases [21]. In order to test the performance of the proposed rotary piston pump in the above grouting process, a visual test system for grouting plugging of the karst pipe is designed. Grouting is performed in the visual test system, considering the impact of the pipe diameter, water velocity, grouting flow rate and other factors (affecting the slurry diffusion and sealing performance). The variation of the parameters was recorded by a real time data acquisition system. This allowed an investigation of the retention mode of the fluids under different moving water conditions. The results of this study have practical significance for slurry blocking and managing pipeline water inrush in karst areas.

Test objectives

(1) Investigate the sealing ability of the piston grouting pump and the rotary piston grouting pump.

(2) Investigate the sealing ability of the two grouting pumps in two different diameter pipe models.

(3) Investigate the sealing capacity of the two grouting pumps at different water flow rates.

(4) Investigate the maximum hydrodynamic retention rate of the slurry based on the theory of minimum deposition rate.

(5) Study the precipitation and migration modes (layer displacement, slip type and suspended type) under the influence of different factors, and identify the criteria for determining the migration mode transition of the slurry.

Test System

The test system utilised in this work consisted of five parts. These are the pipe unit, the stable water supply unit, the monitoring unit, the information unit and the grouting unit. The size of the grouting test system was 5 m × 2 m ×1 m, as shown in Figure 1.

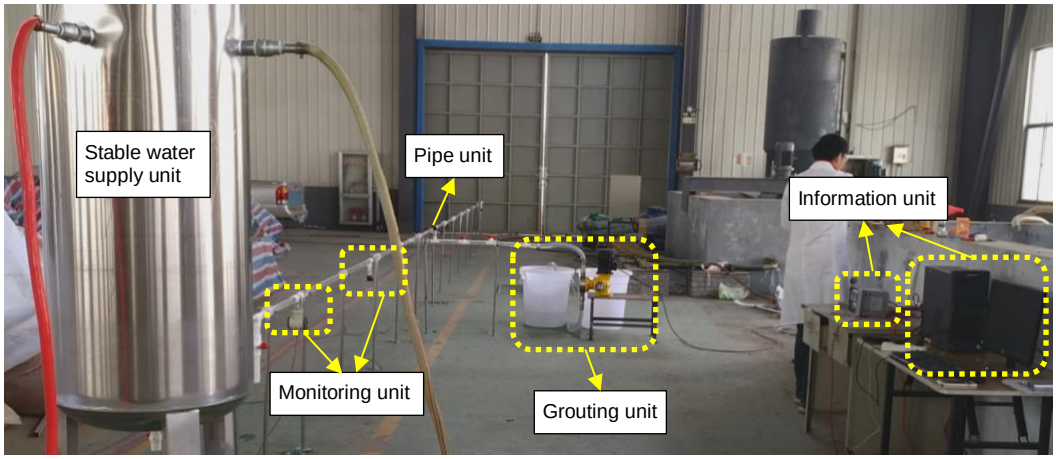

(a)

(b) *(c)* *(d)* *(e)* *(f)*

Fig. 1 – Test system of the grouting equipment; a) overall view of the test system, b) electromagnetic flowmeter, c) Pressure sensor, d) Paperless recorder, e) GM-500 diaphragm pump, f) CN-0.5S rotary piston pump

The pipe unit was equipped with two PMMA (Poly Methyl Methacrylatemethacrylic Acid) pipes (having diameters of 32 mm and 50 mm, respectively). The upstream end of the pipe was connected to the stable water supply unit, which consisted of a storage tank and a control valve.

To control the velocity of the flowing water steadily in the course of the experiment, the water tank was externally connected to the pressure-stabilising air pump. The downstream outlet of the pipeline was connected to the slurry collection container. The monitoring unit included a pressure sensor and an electromagnetic flowmeter. They were located at 6 and 4 m along the pipe, respectively. The variation rules of the pipeline flow and the pressure changes in the flowing water during the grouting process were recorded. The data from the sensors were collected by the information unit, which included an NHR-8100/8700 colour paperless recorder and a computer. The grouting unit included two grouting pumps and two slurry storage barrels.

The proposed CN-0.5S rotary piston grouting pump and the GM-500 mechanical diaphragm pump were used to test the grouting effect. Applying the principle of the triangular rotor engine, the newly developed rotary piston pump changes the cubage of the pump chamber to complete the slurry pumping process through the rotary motion. The rotary piston grouting pump has the advantages of the reciprocating motion of a piston pump. In addition, it relies on high-speed rotation akin to a centrifugal pump. As a result, it can produce both greater pressure and larger output flow. The working principle is shown in Figure 2(a). Each cylinder has two inlets and two outlets. The apex of the rotor divides the cylinder into three working chambers, each of which changes in volume to complete the suction and discharge operations.

The rotor movement is a complex process [22,23], which includes the rotation of the rotor cross-section centroid around the cylinder cross-section centroid. In addition, the rotor's self-rotation is centred on its cross-section centroid. When the power unit causes the main journal of the crankshaft to rotate, the connecting rod neck of the crankshaft drives the inner ring gear on the rotor into a mesh motion with the fixed gear. The rotor rotates around the connecting rod neck at the same time. Therefore, the compound motion of the rotor in the cylinder includes the self-rotation and the revolution of the rotor around the centre of the main journal of the crankshaft. The ratio of the rotor revolution speed to self-rotation speed is 3:1. Therefore, the crankshaft's main journal rotates three times, and three separate cavities accomplish inhalation and discharge twice. In other words, the crankshaft of the main journal rotates once, and a single cylinder completes suction and drainage of two cavities.

The structure of the diaphragm pump is shown in Figure 2(b). In the two symmetrical working chambers of the pump, each chamber is equipped with a flexible diaphragm. The two diaphragms are connected by a connecting rod. The synchronous reciprocating motion of the two diaphragms, driven by the coupling rod, results in cubage changes of the working chambers so as to continuously draw and discharge the liquid.

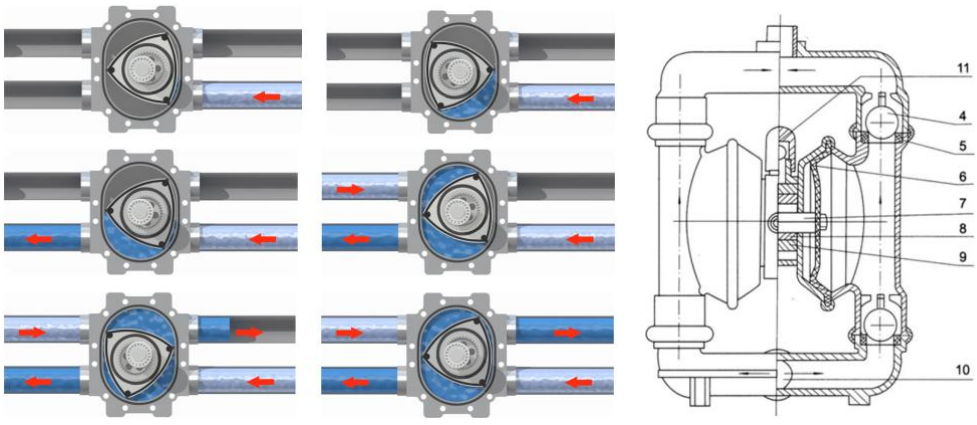

(a) Principle of the rotary piston pump *(b) Principle of a diaphragm pump*

Fig. 2 – Operating principle of the pumps

The theoretical parameters of the CN-0.5S rotary piston grouting pump, and the rated parameters of the GM-500 mechanical diaphragm pump are shown in Table 1.

Tab. 1 - Comparison of parameters of different grouting pumps

Type	Motor power (kW)	Grouting pressure (MPa)	Flow rate (L/min)	Maximum efficiency (%)
CN-0.5S	0.5	0-0.7	0-33.3	79.2
GM-500	0.5	0-0.7	0-8.3	20.2

Test plan

As found from the previous studies, the management of high flow water inrush disaster in karst fissures is limited by the lack of availability of high flow rate grouting equipment. In most cases, methods such as increasing the water–cement ratio, aggregate filling, and chemical slurry were applied. Combined with the previous theoretical research, a grouting test scheme is designed as part of this work. In this test, the pipeline diameter, the moving water flow rate, and the grouting flow rate were focused upon. The thickness of the slurry retained at a fixed monitoring point and the reverse diffusion distance of the slurry were used as the evaluation indices to analyse the plugging effect of the karst pipeline. The role of the grouting flow rate in the karst pipelines was also studied. In this test:

(1) A cement slurry with a water–cement ratio of 1:1 was used for grouting.

(2) Three PMMA pipes with inner diameters of 26 mm (Pipe 1), 44 mm (Pipe 2) and 62 mm (Pipe 3) were used as different pore size karst pipelines.

(3) Each of the PMMA pipes provided different flow velocities, which were 0.1 m/s, 0.2 m/s, 0.3 m/s, 0.4 m/s and 0.5 m/s (Table 2).

(4) At different flow velocities, CN-0.5S was used to provide different grouting flow rates, which were 24 L/min, 26 L/min, 28 L/min, 30 L/min, and 32 L/min. GM-500 was used to provide different grouting flow rates, which were 2 L/min, 3.5 L/min, 5 L/min, and 6.5 L/min.

(5) Grouting was started at 10 s after triggering the timer and was stopped at 85 s. The flow rate and the pressure were recorded at the monitoring points in the grouting process.

In order to ensure identical water flow velocity gradient inside the three pipes, different flow rates were designed (Table 2). The flow rates were controlled by the air pump of the water tank and the electromagnetic flowmeter. The error was controlled within 3%.

Tab. 2 - Flow rates at different flow velocity in each pipe

	Pipe 1	Pipe 2	Pipe 3
Flow velocity（m/s）	Flow rate（L/min）		
0.1	12.74	36.47	72.42
0.2	25.47	72.95	144.85
0.3	38.21	109.42	217.26
0.4	50.94	145.90	289.68
0.5	63.68	182.37	362.10

TEST RESULTS

Analysis of the slurry retention in pipe

When using GM-500 grouting, observation of the retention of the slurry under different grouting flow rates in Pipe 2 showed accumulated slurry at the bottom of the pipe. In addition, there were apparent upper and lower layers of flow water and accumulation. These are shown in Figure 3 (a)–(d). No slurry particles were observed in the upper flowing water. Additionally Figure 3 (a)–(d) shows that with the increase of water velocity, the thickness of the accumulated slurry decreases. In particular, Figure 3 (d) shows that the thickness is 0, indicating removal of the slurry by the flowing water (grouting flow rate: 2.0 L/min, and water velocity: 0.5 m/s).

Figures 3 (e) to (f) show the accumulation states of the slurry using CN-0.5S. The thickness of the accumulated slurry using CN-0.5S is significantly greater than the thickness using GM-500. When the velocity of the flowing water was low, the water in the upper layer was mixed with a large amount of cement granules, as shown in (e). With the increase of the velocity of the flowing water, the cement particles in the upper layer of the water decreased gradually. With the increase of the grouting rate, the thickness of the accumulated slurry increased gradually. Subsequently, the slurry formed many clumps, which rolled and accumulated along the flowing water until the pipe was blocked, as shown in Figures 3 (f) to (h).

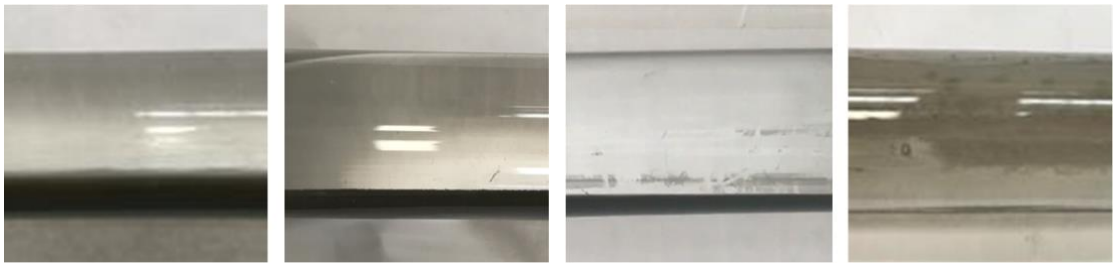

(a) *(b)* *(c)* *(d)*

Fig. 3 – The accumulation of slurry in Pipe 2

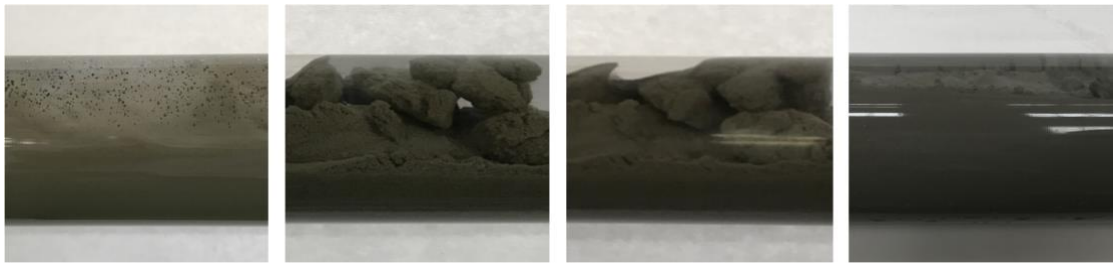

(e) *(f)* *(g)* *(h)*

Fig. 3 – The accumulation of slurry in Pipe 2

The thickness of the accumulated slurry against the velocity of the flowing water is shown in Figure 4. It can also be seen from this figure that the thickness of the accumulated slurry using CN-0.5S was significantly greater than the thickness using GM-500. In Pipe 1, when the grouting rate using CN-0.5S was 32 L/min, the pipe was completely blocked at different water velocity. When the

grouting rate using CN-0.5S was 30 L/min, the pipe was completely blocked when the water velocity was lower than 0.4 m/s. The pipe was not completely blocked when the water velocity was 0.5 m/s, occurring a 1.7 mm top leak. When the grouting rate using CN-0.5S was 28 L/min, the pipe was completely blocked with a water velocity lower than 0.2 m/s. When the grouting rate using CN-0.5S was 26 L/min and 24 L/min, the pipe was completely blocked only when the water velocity was 0.1 m/s. In addition, when the grouting flow rate was 24 L/min, and the water velocity was 0.5 m/s, the maximum top leak appeared at 16 mm using CN-0.5S (about 1/5 of the total thickness). In general, the grouting sealing of CN-0.5S was very effective.

In Pipe 1, the maximum thickness of the accumulated slurry using GM-500 appeared when the grouting flow rate was 8 L/min, and the water velocity was 0.1 m/s, at 16.1 mm. In this case, a top leak of about 2/5 of the total thickness appeared. The accumulation of the slurry for other grouting rates and water velocities was worse, and GM-500 could not achieve effective sealing.

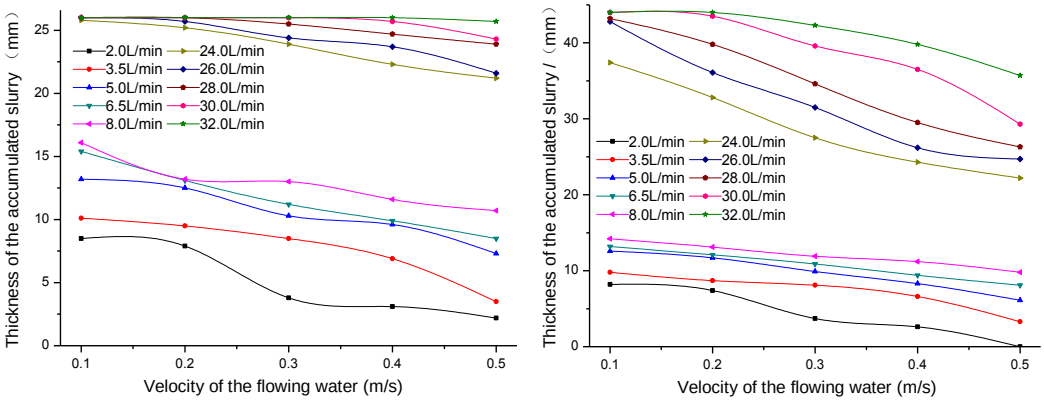

(a) Pipe 1 *(b) Pipe 2*

Fig. 4 – The thickness of the accumulated slurry with the velocity of the flowing water in three pipes

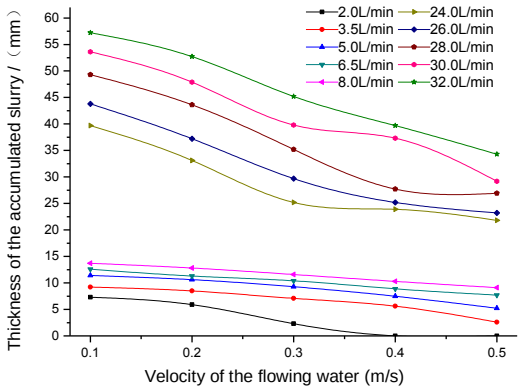

(c) Pipe 3

Fig. 4 – The thickness of the accumulated slurry with the velocity of the flowing water in three pipes

The grouting sealing effect using CN-0.5S was obviously better than GM-500 in Pipe 2 and Pipe 3. The pipe was completely blocked when the flowing water velocity was lower than 0.4 m/s. However, with the increase of the water velocity, the top leak occurred gradually. At the same time,

the top leak was larger using GM-500. This indicates a grouting pump with a larger flow rate is needed to solve the problem.

In general, grouting flow rate is an important factor affecting the sealing performance of the slurry. CN-0.5S indicated better grouting features than that of GM-500.

Analysis of the change of water flow rate under different grouting flow rate

Considering the grouting test in Pipe 2 as an example, different water flow velocities were analysed (at 0.1 m/s, 0.3 m/s and 0.5 m/s). Different grouting flow rates are shown against time in Figure 5.

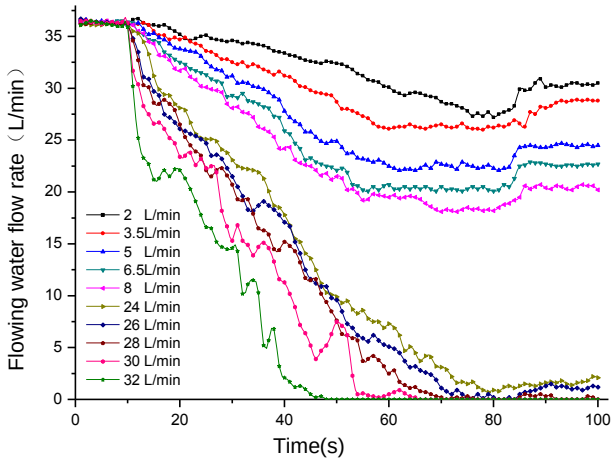

(a) initial flowing water velocity: 0.1 m/s

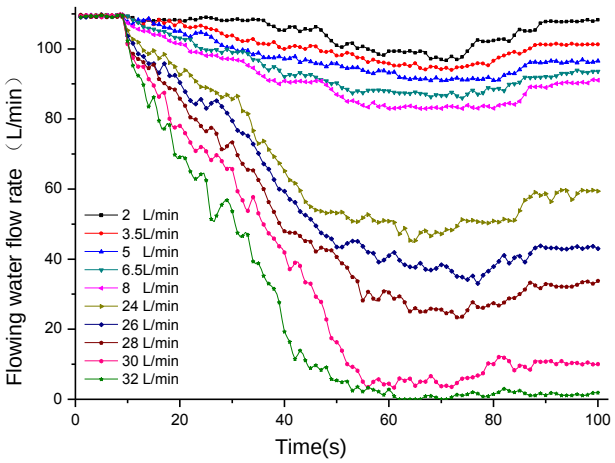

(b) initial flowing water velocity: 0.3 m/s

Fig. 5 – The curve of the flowing water flow rate over time

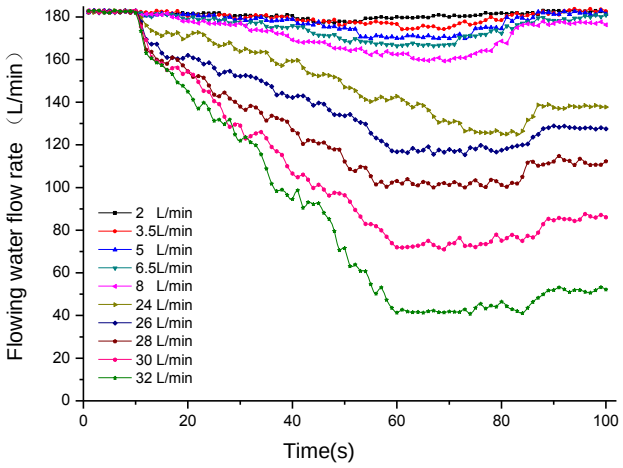

(c) initial flowing water velocity: 0.5 m/s

Fig. 5 – The curve of the flowing water flow rate over time

The following conclusions can be drawn from the above plots:

(1) In case of an identical pipe and an identical initial water velocity, as the grouting flow rate increases, the water flow rate reduces.

(2) In case of an identical pipe and an identical grouting flow rate, the larger the initial motive water flow, the smaller the amount of reduction. The slower the dynamic water flow changes, the greater the difficulty in sealing.

(3) During the grouting process, as the flow rate of the grouting increases, the flow rate of the water decreases gradually. When the grouting is stopped, the water flow rate rebounds. When the grouting flow rate is too small compared with the initial water flow rate, the water flow rate is restored to the initial flow rate.

(4) As shown in Figure 5(a), with an initial water flow velocity of 0.1 m/s and a grouting flow rate higher than 24 L/min (i.e., grouting using CN-0.5S), the flowing water could be sealed effectively. Figure 5(b) shows a case with an initial water flow velocity of 0.3 m/s and a grouting flow rate of 32 L/min, providing effective water sealing. Figure 5(c) shows a case where an initial water flow velocity of 0.5 m/s and a grouting flow rate of 32 L/min caused a reduced water flow rate, but could not seal it effectively. The grouting flow rate needed to be increased in this case.

(5) From the above four points it can be deduced that the flow rate of the grouting pump plays a key role in the effective sealing of flowing water.

Analysis of the performance of CN-0.5S and GM-500

The monitored parameters of CN-0.5S and GM-500 in Pipe 2 were used to evaluate their performances. With a water flow rate of 0.5 m/s, and initial grouting flow rate of 32 L/min and 8 L/min (respectively for CN-0.5S and GM-500), the dynamic curves of the grouting flow rates for CN-0.5S (q_1) and GM-500 ($q_{2)}$ with time (t), and the differential pressures between the inlet and outlet are shown in Figure 6.

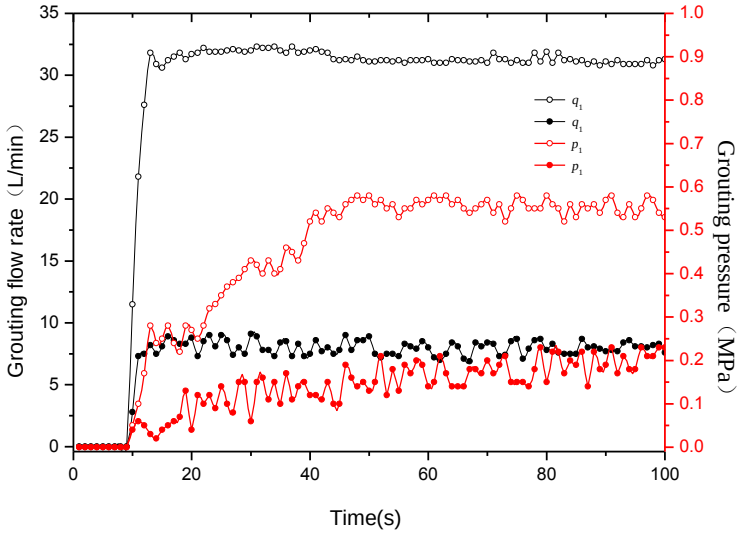

Fig. 6 – The flow and pressure changes over time

From the above flow rate and differential pressure curves, it can be observed that:

(1) The flow rate and differential pressure of CN-0.5S were relatively stable with time, and the flow rate and differential pressure of GM-500 fluctuated significantly with time. The data after 8 s was selected to calculate the maximum flow rate (Q_{max}), the minimum flow rate (Q_{min}) and the average flow rate (Q_m) of CN-0.5S and GM-500. The results are as follows:

Tab. 3 - Flow characteristic value

Pump	Q_m (L/min)	Q_{max} (L/min)	Q_{min} (L/min)
CN-0.5S	31.4	32.3	30.6
GM-500	8	9.1	6.9

The fluctuation in the flow rate can be expressed by the non-uniform coefficient given by:

$$\delta Q = \frac{Q_{max} - Q_m}{Q_m} \times 100\% \quad (1)$$

Here, δQ is the non-uniform coefficient of the flow rate.

Using the data of Table 4 in Equation 1, the non-uniformity coefficients of the flow rate for CN-0.5S and GM-500 are found to be 2.9% and 13.8%, respectively. It can be seen that the stability of output for CN-0.5S is better than that of GM- 500.

(2) According to the differential pressure and flow rate, the expression of the head is given by:

$$H = \frac{p}{\rho g} + \frac{v_2 - v_1}{2g} \quad (2)$$

Here, H is the head of CN-0.5S, p is the differential pressure of the inlet and outlet; ρ is the density of the medium, g is the acceleration due to gravity, v_2 is the flow velocity at the outlet, and v_1 is the flow velocity at the inlet.

The flow velocity of the inlet and outlet can be obtained by the flow rate at these locations and the corresponding cross-sectional areas. The efficiency of the universal joint between the motor and the test pump shaft is 98%. The efficiency of CN-0.5S can be expressed as:

$$\eta = \frac{\rho g H_m Q_m}{0.98 P_0} \tag{3}$$

Here, η is the efficiency of the test pump, H_m is the average of the head of the test pump, and P_0 is the power of the motor.

The efficiency of CN-0.5S and GM-500 were obtained using the above expressions and were calculated at 51.27% and 4.08%, respectively. Evidently, the efficiency of CN-0.5S in the karst pipeline grouting test is significantly greater than that of GM-500.

ENGINEERING APPLICATION

Engineering background

The test area was located in a dam tunnel in Xiangxi Tujia and Miao Autonomous Prefecture in Hunan Province. The terrain of the tunnel was relatively high, the surrounding mountains were thick in vegetation, and the catchment area was large. The area has a subtropical monsoon humid climate zone with abundant, concentrated and high-intensity rainfall. The average annual rainfall is 1326.3–1468.4 mm. The maximum rainfall is 1992.7 mm. Separated by YK86+080 to YK86+200, the catchment area is large. After a precipitation, a large amount of surface water passes through the dissolution fractures and the fault fracture zones along the slopes into the tunnel. A large amount of groundwater infiltration causes the lining of this section to crumble and the floor moves up. The project safety was in question, and the construction progress was affected seriously. During a period when the first spray had been completed, but the second lining had not yet been constructed, a large amount of high-current water gushed in through the tunnel entrance right hole section (YK86+140–YK86+200). The maximum water flow rate reached 4.14 m^3/s, and water inrush continued for 4-5 days, which gradually declined in subsequent. This event caused damages to some of the initial spray. The surrounding rock was partially floated up. Using a combination of high-density electrical profiling and drilling exploration, water infiltration diagrams at the tunnel vault, the right wall and the floor were developed. These are shown in Figure 7.

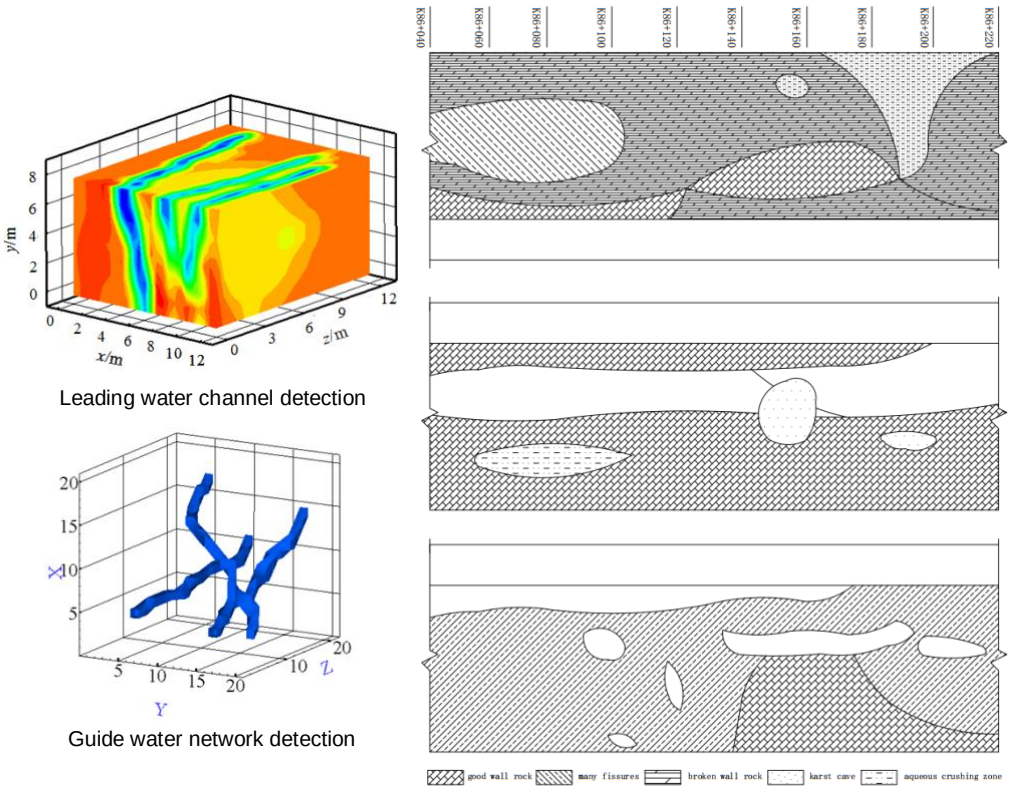

Fig. 7 – Tunnel surrounding rock environment detection

The affected section had two faults, F2 and F6. The F2 fault slanted to the southeast with an inclination of 35°–45°, and it chamfered the tunnel at YK86+130. The width of the crushed zone was 15~30 m. This affected the tumour-like limestone, created numerous karst fractures, caves and crushed rocks. The general fault orientation of F6 was toward the southeast with an inclination of 40°–45°. This fault caused disturbances along the slope and chamfered the tunnel at YK86+025. The width of the crushed zone was 15–20 m. The rocks of the two fault fractures and the affected zones went through slight silicification, mylonitisation and obvious chloritisation. The rock mass is mainly composed of fragmentation structures, influenced by tectonics, and karst, where jointed fractures develop. The presence of strong weathering shale in the limestone, make them fragile and prone to collapse during excavation. The stability of surrounding rock is poor.

In summary, this tunnel section is characterised by karst fissures and karst caves, close spatial relationships, strong hydraulic conductivity, diverse gushing water types, regionalisation and wide spatial distribution of inflow points. Strong surface precipitation and groundwater flow into the tunnel through the karst fissures and caves, thus constituting the main source of gushing water into the tunnel.

Grouting test on site

Using the results of the previous explorations, the centralised gushing channel and the large karst water storage structure area were chosen as the experimental sections. By using the traditional piston grouting pump 3SNSA, and the newly designed grouting equipment CN-1.5S (discussed in this paper), the same-hole grouting and different-hole synchronous grouting tests were carried out. The performance parameters are listed in Table 4. In the process of grouting, single-liquid grout was mainly used. The dynamic grouting material was GT-1, and the single-grout

water–cement ratio was adjusted to 0.8:1–1:1 dynamically according to the thickness of the liquid leakage. As the first and the second lining of the tunnel had been completed, backwall grouting was adopted in order to prevent secondary damage to the lining structure caused by the grouting pressure, and the final grouting pressure was designed to be 2 MPa. During the process of grouting, the grouting pressure and grouting flow rates were collected in real time. A three-parameter logger was used to obtain the data during the whole grouting process using a common grouting pump and new rotary piston grouting pump. Finally, the grouting quantity of every drill hole and grouting time were analysed.

(a) Piston pump *(b) Rotary piston pump*

Fig. 8 – Two types of grouting pumps

Tab. 4 - The parameters of the two grouting pumps

Type	Motor power (kW)	Grouting pressure (MPa)	Grouting flow rate (L/min)
CN-1.5S	18.5	0-6	0-536.2
3SNSA	18.5	0-10	0-207

Test results and analysis

(1) Single-hole sequential grouting

A single liquid cement slurry was used to fill the cavity in the exposed single drilling hole ZW4-12 and ZW5-13, and the final pressure was 1.5 MPa. In the process of grouting, 3SNSA was used for grouting initially. After grouting for days, the amount of grouting did not decrease, and the grouting pressure did not increase. In this case, CN-1.5S was used for grouting and filling. The sealing of the cavity was completed in a short period of time. The total amount of grouting and grouting pressure is shown in Figure 13. For the ZW4-12 hole, 3SNSA was used for grouting during the first 6 days. The daily grouting volume did not change significantly, and the grouting pressure was consistently low. After using CN-1.5S, the daily grouting surged, and the grouting pressure reached the final designed pressure on the 3rd day.

(2) Separate-hole synchronous grouting test

The drilling hole ZJ8-16 and ZJ8-16 were exposed revealing the karst fissure pipeline and the water inflow was large. GT-1 double liquid cement slurry was used to seal the gushing water, and the final design pressure was 2 MPa. 3SNSA and CN-1.5S were used in ZJ10-12 and ZJ8-16, respectively, and grouting treatment was started at the same time. The daily grouting amount and

grouting pressure changes are shown in Figure 14. The daily grouting amount was significantly higher in the ZJ10-12 grouted by CN-1.5S than that of the ZJ8-16 grouted by 3SNSA. ZJ10-12 reached the designed final pressure in 3 days with CN-1.5S. The cumulative amount of grouting was 453 m^3. The drilling of ZJ8-16 continued to reach the designed final pressure in 7 days, with a cumulative grouting volume of 470 m^3.

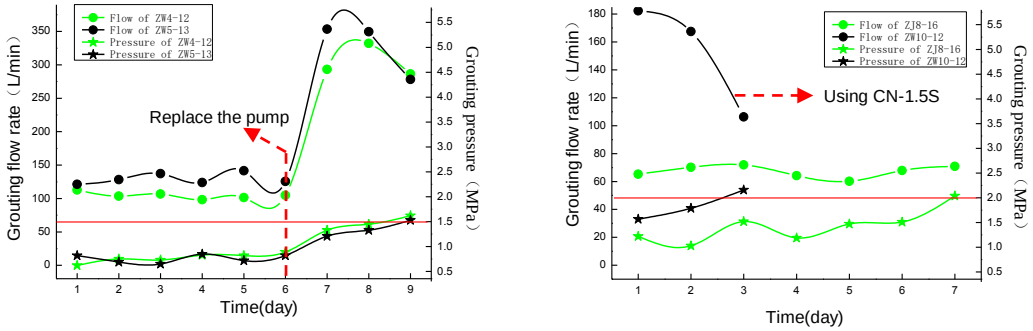

(a) Single-hole grouting *(b) Separate-hole grouting*

Fig. 9 – The changes of grouting flow rate and grouting pressure

Grouting effect

It can be observed from the grouting tests that the grouting flow rate of the new rotary piston pump is significantly higher than that of the existing grouting equipment, such as grouting filling in karst water storage structures or grouting sealing with low-pressure flowing water. The grouting efficiency is also considerably improved. After further adaptation of the newly developed grouting equipment in the overall test sites, the right hole of the tunnel reached the management requirement on October 15, 2015. The surrounding rock and lining were found to be intact. The entire right hole grouting project was 28 days ahead of the schedule, saving approximately 30% of the resources. A visual comparison of the test site before and after the grouting work can be seen in Figure 10.

(a) Before the grouting *(b) After the grouting*

Fig. 10 – The comparison before and after the grouting engineering

CONCLUSION

In this study, a new type of grouting pump is proposed supported by a comparative grouting test carried out against existing grouting pumps. In the test, two kinds of PMMA pipes were chosen to simulate two kinds of karst pipes. CN-0.5S and GM-500 were used for grouting sealing tests at different grouting flow rates. The test results indicate that:

(1) The thickness of the accumulated slurry using CN-0.5S is significantly greater than the thickness using GM-500 at the same monitoring points in each pipe.

(2) In Pipe 1 and Pipe 2, CN-0.5S can realise the complete sealing of the flowing water.

(3) With the same pipe diameter and the same initial flowing water velocity, an increase in the grouting flow rate causes significant reduction in the water velocity. The flow rate of the pump plays a key role in effectively blocking the flowing water.

(4) By recording various parameters of the grouting pump, the mean value of the grouting pressure and grouting flow rate of CN-0.5S was found to be larger than that of GM-500. The operational efficiency of CN-0.5S is far greater than that of GM-500.

In a practical engineering application, the newly developed rotary piston pump CN-1.5S and a traditional piston pump 3SNSA were tested in single- and separate-hole grouting experiments. The following conclusions were drawn:

(1) In the single-hole grouting, after changing CN-1.5S, the grouting flow rate increased greatly, and the target pressure of the design was quickly achieved.

(2) In the separate-hole grouting, the hole using CN-1.5S achieved the design pressure within half the allocated time compared to the hole using 3SNSA.

In summary, it can be stated that the newly developed rotary piston grouting pump has a high flow rate and high efficiency, which allows the faster completion of grouting engineering tasks and the reduction of the associated costs.

ACKNOWLEDGEMENTS

This work is supported by the Natural Science Foundation of Shandong Province, China (ZR201702230205), the Key Project of Chinese National Programs for Fundamental Research and Development (973 Program) (2013CB036000).

REFERENCES

[1] Xu Z. H., Li S. C., Li L. P., Chen J.,Zhang Z. G. and Shi S. S., 2011. Cause, disaster prevention and controlling of a typical kind of water inrush and lining fracturing in karst tunnels. Chinese Journal of Rock Mechanics and Engineering, vol. 30, no. 7: 1396-1404.

[2] Li S. C., Shi S. S., Li L. P., Chen J., Xu Z. H., Zhou Z. Q. and Yuan Y.C., 2014. Control of water inrush in typical karst tunnels in three gorges reservoir area and its application. Chinese Journal of Rock Mechanics and Engineering, vol. 33, no. 9: 1887-1895.

[3] Li S. C., Li S. C., Zhang Q. S., Xue Y. G., Ding W. T., Zhong S. H., He F. L. And Liu Y. S., 2007. Forecast of karst-fractured groundwater and fefective geological conditions. Chinese Journal of Rock Mechanics and Engineering, vol. 26, no. 2: 217-225.

[4] Sun Q., Zhu S. Y. and Zhang R., 2013. Analysis on Water Inrush Mechanism of Pipeline Conduction. Chinese Journal of basic science and engineering, vol. 21, no. 3: 463-470.

[5] Li L. P., Li S. C. and Zhang Q. S., 2010. Study of mechanism of water inrush induced by hydraulic fracturing in karst tunnels. Rock and Soil Mechanics, vol. 31, no. 2: 523-528.

[6] Xue Y. G., Li S. C., Su M. X., Li S. C., Zhang Q. S., Zhao Y. and Li W. T., 2011. Study of geological prediction implementation method in tunnel construction. Rock and Soil Mechanics, vol. 32, no. 8: 2416-2422.

[7] Yuan J. Q., Chen W. Z., Huang S. W., Zhou X. S., Zhou Z. H., and Liu J. Q., 2016. Mechanism and synergetic treatment technology of water inrush disaster in completely and strongly weathered granite tunnels. Chinese Journal of Rock Mechanics and Engineering, vol. 35, supp. 2: 4164-4171.

[8] Wang X. Y., Tan Z. S., Wang M. S., and Zhang M., 2008. Analysis of interaction between surrounding rock and lining in high water-level tunnels with controlled drainage. Rock and Soil Mechanics, vol. 29, no. 6: 1623-1628.
[9] Liu S., Li X., Sun T., and Zhang H., 2016. Calculation of the Hydraulic Extension Limit of an Extended-Reach Well with Allowance for the Power Limitations of the Available Mud Pumps. Chemistry and Technology of Fuels and Oils, vol. 51, no. 6: 713-718.
[10] Xia J. M., Liu H. B., Zhang Z. H., ZHU S. J. and YU X., 2016. Vibration Analysis of the Crank-link Mechanism of Reciprocating Bilge Pumps. Noise and Vibration Control, vol. 36, no. 3: 151-154.
[11] Yan X. A., Zheng W., Zhang Q., and Lu B. X., 1999. Finite Element Analysis on the Structural Vibration of the Discharge Pipes for Reciprocating Pumps. Chinese Journal of Mechanical Engineering, vol. 35, no. 6: 74-76.
[12] Wu H., Tong Z. W., Chen H. and Liang J. S., 2014. Dynamic simulation analysis on improved mud pump BW-280/12 using SolidWorks motion and ADAMS. Manufacturing Automation, vol. 19, no. 5: 65-66.
[13] Zhang C., Feng S. B., Bai Q. P., and Ai Z. H., 2015. The Development of a Test Bench for Testing the Hydraulic Pump with High Pressure Large Flow. Hydraulics Pneumatics & Seals, no. 7: 82-84.
[14] Song R. G., Zhang B. H. and Yang Y. X., 2007. Study on the meshing characteristic of a new cycloidal pump. Powder Metallurgy Technology, vol. 25, no. 2: 99-103.
[15] Ren H. Y., Zhang S. C., Wang Z. H., Deng H. Y., Zhou S. B. and Xu Y. Y., 2011. Analysis of the Characteristics and Flow Rate of a New Eccentric and Squirmy Rotor pump for Cleaning Machine. Light Industry Machinery, vol. 29, no. 2: 14-17.
[16] Li Y. L., Liu K. and Peng J. H., 2006. Research and Development on Integrative Parameterization Design with Its Solid Model for Cycloid Pump. Transactions of the Chinese Society for Agricultural Machinery, vol. 37, no. 12: 109-113.
[17] Chen Z. B., Zou Y. Z., Jiang Z. and Dai M., 2017. Numerical Simulation of the Effect of the Gap between Rotor and Pump on the Performance of the Rotor Pump. Noise and Vibration Control, vol. 37, no. 2: 62-66.
[18] Xu B., Hu M., Zhang J. H. and Su Q., 2016. Characteristics of volumetric losses and efficiency of axial piston pump with respect to displacement conditions. Journal of Zhejiang University SCIENCE A, vol. 17, no. 3: 186-201.
[19] Yan P., Li S. Y., Yang S., Wu P. and Wu D. Z., 2017. Effect of stacking conditions on performance of a centrifugal pump. Journal of Mechanical Science and Technology, vol. 31, no. 2: 689-696.
[20] Wen D., Chen F., Zhen X. S., Chai W. C., Wang J. and Zhou C., 2016. Analysis of Leakage and Volumetric Efficiency for Cam-Rotor Double-Stator Vane Pump. Journal of Xi'an Jiaotong University, vol. 50, no. 9: 20-24.
[21] HU W., 2013. Grout diffusion and plugging mechanism in rockmass channel and fissures under hydrodynamic condition[Ph. D. Thesis]. China University of Mining and Technology.
[22] LI S. C., Li M. T., Zhang X., Zhang Q. S., Hao P. S. and Wang Z. A., 2018. Investigation on Performance of Triangular Rotor Pump Based on Numerical Simulation and Experiment. Transactions of the Chinese Society for Agricultural Machinery, vol. 49, no. 9: 389-396.
[23] LI M. T., LI S. C., Zang X. and Zhang Q. S., 2018. Experimental investigations on extrusive eccentric rotary pump. Journal of Harbin Institute of Technology, 2018-03-26.